Soft Matter

PAPER

View Article Online
View Journal | View Issue

Cite this: *Soft Matter*, 2015, **11**, 741

Solvent-mediated gel formation, hierarchical structures, and rheological properties of organogels†

Ming-Ming Su,‡[a] Hai-Kuan Yang,‡[ab] Li-Jun Ren,[a] Ping Zheng[a] and Wei Wang*[a]

Received 2nd November 2014
Accepted 15th November 2014

DOI: 10.1039/c4sm02423k

www.rsc.org/softmatter

We report the formation of solvent-mediated gels as well as their hierarchical structures and rheological properties. The gelator used is a hybrid with a molecular structure of cholesterol–polyoxometalate–cholesterol, in which the cholesterol dissolves well in toluene and *N*,*N*-dimethylformamide (DMF), whereas the polyoxometalate cluster dissolves only in DMF. These solubility differences enable the gelator to form thermally reversible supramolecular organogels by mixing solvents of toluene and DMF when the volume fraction, f_{tol}, of toluene is larger than 85.7 v/v%. We found a V-shaped correlation between the gelation times, t_{gel} and f_{tol}: t_{gel} decreases from 1300 min to 2 min when f_{tol} increases from 85.7 v/v% to 90.0 v/v%. It then increases from 2 min to 5800 min when f_{tol} further increases from 90.0 v/v% to 100.0 v/v%. We observed ribbon-like self-assembled structures in the gels as well as a structural evolution from rigid and straight ribbons to twistable ones from f_{tol} = 85.7 v/v% to f_{tol} = 100.0 v/v%. These ribbons constitute two three-dimensional (3D) gel networks: one is constructed *via* physical connection of the rigid and straight ribbon, and the other is built up from ribbons splitting and intertwining. The latter has a better 3D gel network that offers improved rheological properties. Fundamentally, this solvent-mediated approach regulates the balance between solubility and insolubility of this gelator in the mixing solvents. It also provides a new method for the preparation of organogels.

Introduction

Over the last few decades, the intense study of supramolecular gels derived from low molecular mass (LMM) organic gelators containing smart and functional moieties has developed into a well-recognized field of a multidisciplinary science. The goal is to develop novel soft functional materials for applications in biomaterials, catalyzers, electronic devices, templates for nanostructures, drug carriers, and oil recovery.[1–13] Supramolecular gels are normally formed through non-covalent interactions such as hydrogen bonds, π–π interactions, coordination bonds and van der Waals forces. This offers an alternative to thermo-reversible gels with the diversity of hierarchical nanostructures derived from molecular self-assembly.

Supramolecular gels are usually prepared by heating LMM organic gelators in an appropriate solvent to form a supersaturated solution followed by cooling. While cooling, the molecular condensation can form amorphous aggregates, ordered aggregates that can propagate similarly to crystals, or aggregate intermediates between these two. Each has different structural orderings of varying length scales. Their formation greatly depends on the conditions used. Previous studies demonstrated clearly that the solutions gel once the aggregate intermediates further construct a three-dimensional (3D) gel network. This is a molecular self-assembly process, during which the primary, secondary, and tertiary supramolecular structures form in a step-by-step manner.[5] Therefore, the gelation process of a gelator and the performances of its gels thoroughly depend on the formation of these hierarchically self-assembled structures. In other words, the gelation process and performances of a gel can be regulated if the forming process and perfection of the hierarchical structures can be manipulated purposefully and in a programmed way. One must delicately balance the solvent–gelator interactions and gelator–gelator interactions by rationally designing the molecular structures of LMM gelators as well as purposefully adjusting the dissolving capacity of solvents.[10] In fact, this balance can be also mediated by means of mixing two or more solvents with different gelator solubilities.[14–21]

Polyoxometalates (POMs) are nanoscale polyanionic clusters of early transition metals with attractive functionalities.[22,23] Their organic functionalization has created a large number of new POM-containing hybrids for widespread applications.[23,24]

[a]*Centre for Synthetic Soft Materials, Key Laboratory of Functional Polymer Materials of the Ministry of Education, Institute of Polymer Chemistry, Nankai University, Collaborative Innovation Centre of Chemical Science and Engineering (Tianjin), Tianjin 300071, China. E-mail: weiwang@nankai.edu.cn*

[b]*Department of Chemistry, North University of China, Taiyuan, Shanxi 030051, China*

† Electronic supplementary information (ESI) available. See DOI: 10.1039/c4sm02423k

‡ These authors contributed equally to the study.

POM-containing hybrids can form interesting nanomaterials or nano-objects with rich self-assembled structures because the POMs have large differences in function and property from the different organic moieties.[25–29] These hybrids can also form POM-containing gels.[30–36]

Recently, our group prepared and studied organogels from the hybrid gelators constructed from organically functionalized POM clusters.[35,36] Our target is to develop novel functional soft materials for potential applications in catalysis, biology, and materials science because the nanoscale anionic metal–oxygen clusters possess a diverse range of properties and attractive functionalities. The hybrid gelators have molecular structures of organic moiety–POM–organic moiety. The solubility of the organic moieties is markedly different from that of the POM clusters in the organic solvents.

In our first study, we prepared a POM-containing hybrid gelator composed of two second-generation alkyl-group-modified poly(urethane amide) (PUA) dendrons and an organically modified Anderson-type POM cluster. We found that the gelator could form a stable organogel at room temperature in *N*,*N*-dimethylformamide (DMF).[29] Multiple hydrogen bond interactions of the PUA dendrons and interactions of the POM clusters drove the formation of the ribbon-like supramolecular structures. This work demonstrated the concept of softening POM clusters. In our second work, we presented an intriguing phenomenon: the toluene organogels of a cholesterol–POM–cholesterol hybrid could not be converted into the solutions when reheated to 120 °C, which is *ca.* 10 °C higher than the boiling point (110.8 °C) of toluene.[36] We found an orderly arranged POM layer sandwiched between two cholesterol layers in supramolecular ribbons. We thought that the interactions of the POM clusters were maximized and that the ribbons become thermally stable at 120 °C. This work demonstrated another concept of creating organogels with an enhanced thermal stability by rationally designing a gelator and controlling its self-assembled structures.

Herein, we describe the gelation process of the cholesterol–POM–cholesterol gelator and the performances of its organogels within mixed solvents of toluene and DMF. We are motivated by a fact that there is a large difference in solubility of the two building blocks: toluene and DMF are good solvents for cholesterol, and DMF is a good solvent for the POM. We used a solvent-mediated method to regulate the balance between solubility and insolubility of this gelator in the mixed solvents by altering the toluene/DMF volume ratio. We further show that the solvent mediation can regulate hierarchically self-assembled structures as well as their growth rate. Therefore, we observed great changes in the gelation time within a wide range of time scales and different rheological properties of the gels.

Experimental section

Materials

The details of its synthetic procedure of the hybrid gelator have been reported in our previous study[37] and are summarized in the ESI.† The solvents used in this work are analytical grade *N*,*N*-dimethylformamide (DMF) and toluene, purchased from Beijing Chemical Reagent Industry. They were dried and freshly distilled prior to use.

Gel preparation and gelation test

Toluene gel. A known weight of the gelator and a known volume of toluene were placed into a screw-cap vial. Then, the sealed vial was placed into a heating vacuum oven (Binder model: VD23), of which temperature was pre-set at 80.0 °C. At this temperature, the gelator dissolved into toluene to form a clear solution with a concentration $c = 10.0$ mg mL^{-1}. The solution in the vial was cooled to about 23.0 °C in a heating vacuum oven, of which temperature was reset at 23.0 °C. The vial-inversion method[38] was used for appraisement of its gelation. The gelation time was determined when the solutions became immobilized.

Toluene/DMF gels. At first, a known weight of the hybrid gelator and a known volume of the DMF were placed into the screw-cap vials at room temperature. By gently shaking, the gelator dissolved in DMF to form a clear solution. Then, a certain amount of toluene was added into the DMF solutions to the predetermined concentration ($c = 10.0$ mg mL^{-1}) and the toluene fractions. After staying for a few minutes, hours or days in the oven, of which temperature was pre-set at 23.0 °C, the solutions became immobilized and the gelation time was determined by the vial-inversion method.

Characterizations

X-ray diffraction (XRD). The XRD experiment was conducted with a Rigaku D/Max-2500 X-ray diffractometer, equipped with a Cu-Kα radiation ($\lambda = 0.154$ nm) source operated at 40 kV/100 mA. The organogels were dried in a vacuum oven (Binder model: VD23) and preset to 30.0 °C for 24 hours, and then, the dried gels were crushed into powder. The powder samples were used directly for XRD characterization.

Atomic force microscopy (AFM). AFM images were recorded using a multi-model atomic force microscope (Digital Instrumental Nanoscope IV) in tapping mode. The samples for AFM characterization were prepared by slightly touching the gels onto a freshly peeled-off mica surface and then dried under vacuum at 23.0 °C for 24 hours.

Oscillatory rheology. The dynamic shear storage and loss moduli (G' and G'') of our organogels were determined using an Anton Paar MCR302 rheometer under a strain sweep condition with a constant frequency of 10.0 Hz. The CP50-1 cone-plate geometry with a 50 mm plate diameters and a 1° cone angle was used. The 0.1 mm thick sample covered the entire plate.

Results and discussion

Hybrid structure of gelator

As shown in Scheme 1, the gelator is an organo-POM hybrid constructed by further functionalization of an organically functionalized Anderson-type polyoxomolybdate $(Bu_4N^+)_3\{(MnMo_6O_{18})^{3-}[(OCH_2)_3CNH_2]_2\}$[39,40] using two *o*-succinyl-cholesterols. It is denoted as cholesterol–POM–cholesterol in this study. The molecular dimension of the

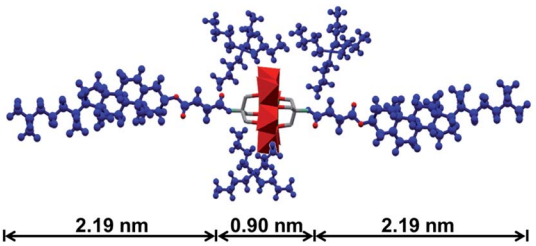

Scheme 1 Synthetic route and structure of the hybrid gelator. Note that the POM cluster is encapsulated by three tetrabutyl ammonium cations (Bu_4N^+).

hybrid gelator was estimated using the ChemDraw software (MM2 force field) and Diamond software from the reported crystallographic data.[39] The molecular length is about 5.3 nm and the diameter of the POM cluster is 0.75 nm.

Solubility and gelation

This hybrid consists of two nonpolar cholesterol parts and one polar POM cluster. They have different solubilities. The cholesterol parts dissolve in toluene and DMF, whereas the POM cluster dissolves only in DMF. The hybrid can dissolve into DMF at room temperature and into toluene at 80 °C. This difference may be due to interactions between the polar POM clusters that are stronger than those between the nonpolar cholesterol parts. When the hot toluene solution was cooled to 23.0 °C, it gelled into a stable POM-containing organogel with a well-defined 3D network of self-assembled nano-ribbons.[36] This gelation process may take days or weeks and is highly dependent on concentration and temperature. For instance, the gelation time is $t_{gel} \approx 5800$ min at $c = 10.0$ mg mL^{-1} at 23.0 °C. However, the DMF solution cannot form a gel under the same conditions.

Nonpolar toluene has a dielectric constant $\varepsilon^e = 2.24$, whereas polar aprotic DMF has $\varepsilon^e = 36.71$. In this work, we regulate the gelation process of this hybrid gelator by adjusting the volume fraction, f_{tol}, of toluene in the mixed solvents. In Table 1, we summarize the dielectric constant, ε^e, of the mixed solvents, the phase behavior and t_{gel} of the solutions as a function of f_{tol}. The dielectric constants of the mixed solvents were calculated using $\varepsilon^e = \varepsilon^e_{tol} f_{tol} + \varepsilon^e_{DMF} f_{DMF}$, in which ε^e_{tol} and ε^e_{DMF} are the dielectric constants of toluene and DMF, respectively. The dielectric constant of the mixed solvents can be adjusted from $\varepsilon^e = 36.71$ for pure DMF to $\varepsilon^e = 2.24$ for pure toluene.

Within $0 \leq f_{tol} < 85.7$ v/v%, we only observed a solution of the hybrid, corresponding to $\varepsilon^e = 36.71$ to $\varepsilon^e = 7.17$. Because $f_{tol} \geq 85.7$ v/v% and $\varepsilon^e \geq 7.17$, the solutions started to gel. At $f_{tol} = 85.7$ v/v%, $t_{gel} = 1300$ min. When f_{tol} is slightly higher than 85.7 v/v%, t_{gel} decreases significantly. For instance, $t_{gel} = 20$ min at $f_{tol} = 87.5$ v/v%. Intriguingly, $t_{gel} = 2$ min at $f_{tol} = 90.0$ v/v%. Therefore, a solution could be converted into a gel when a few drops of toluene were added into the DMF solution and the vial was gently shaken by hand. More intriguingly, t_{gel} increases when $f_{tol} > 90.0$ v/v%. At $f_{tol} = 100.0$ v/v%, $t_{gel} = 5800$ min.

Table 1 Dielectric constant, ε^e, of the mixed solvents and phase behavior and t_{gel} of the solutions at $c = 10.0$ mg mL^{-1} as a function of f_{tol}[a]

f_{tol} (v/v%)	ε^e	Phase	t_{gel} (min)
0	36.71	S	—
50.0	19.48	S	—
66.7	13.72	S	—
75.0	10.86	S	—
80.0	9.13	S	—
83.0	8.01	S	—
85.7	7.17	G	1300
87.5	6.54	G	20
88.8	6.10	G	5
90.0	5.68	G	2
91.0	5.34	G	8
93.0	4.65	G	50
95.0	3.96	G	300
97.0	3.27	G	1500
99.0	2.58	G	4300
100.0	2.24	G	5800

[a] S and G denote solution and gel phases.

Fig. 1 clearly shows a correlation between t_{gel} and f_{tol} of the organogels in the toluene/DMF mixed solvents at $c = 10.0$ mg mL^{-1} and 23.0 °C. The images show a sol at $f_{tol} = 85.0$ v/v% (a), gels at $f_{tol} = 90.0$ (b), and 100.0 v/v% (c). At $f_{tol} = 85.7$ v/v%, the solution becomes gel-like. This means that a change in the solvent solubility of the gelator in the mixed solvents causes a sol–gel transition. This figure displays a V-shaped f_{tol}-dependence of t_{gel}. The t_{gel} decreases from 1300 to 2 min for $f_{tol} = 85.7$ v/v% to $f_{tol} = 90.0$ v/v%, and increases from 2 to 5800 min for $f_{tol} = 90.0$ v/v% to $f_{tol} = 100.0$ v/v%. This V-shaped f_{tol}-dependence and the t_{gel} variability over time scales spanning two orders of magnitude are rarely found in gelation studies.

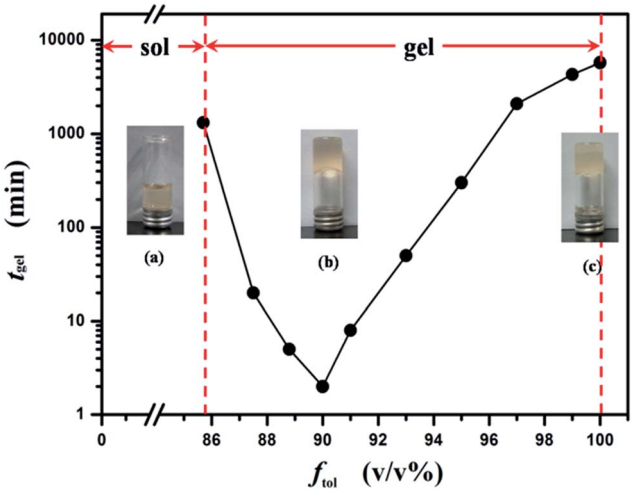

Fig. 1 Gelation time, t_{gel}, of the organogels as a function of f_{tol} in the mixed solvent of toluene and DMF at $c = 10.0$ mg mL^{-1}. The images show a sol at $f_{tol} = 85.0$ v/v% (a), gels at $f_{tol} = 90.0$ (b), and 100.0 v/v% (c).

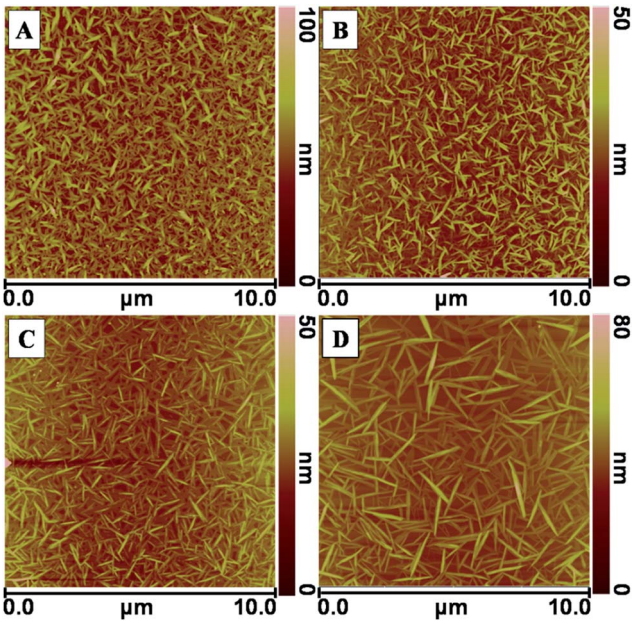

Fig. 2 AFM images of the dried xerogel samples of the organogels at $c = 10.0$ mg mL^{-1} and different f_{tol} in the toluene/DMF solvents. (A) $f_{tol} = 85.7$ v/v%, (B) $f_{tol} = 87.5$ v/v%, (C) $f_{tol} = 88.0$ v/v%, and (D) $f_{tol} = 90.0$ v/v%.

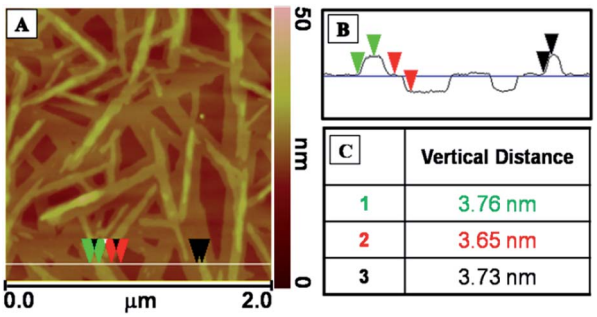

Fig. 3 (A) Enlarged AFM image showing ribbon-like aggregates of the dried xerogel sample of the organogel at $f_{tol} = 90.0$ v/v%. The white line shows a section for a height profile measurement. (B) Height profile of the ribbons. (C) Vertical distance (or height) of the ribbons.

Morphology and structure of assemblies

To better understand the differences in the gelation process of these organogels in the mixed solvents, we performed a study on the morphology and structure of the supramolecular assemblies in dried xerogel samples using AFM. The height images in Fig. 2 show a mass of the straight and elongated assemblies found in the samples of the organogels from $f_{tol} = 85.7$ v/v% to $f_{tol} = 90.0$ v/v%. Their formation indicates that an anisotropic growth occurred. Seemingly, they did not form an intertwined 3D gel network. Further characterization at $f_{tol} = 90.0$ v/v% displays the fine structure, as shown in Fig. 3. The enlarged image in Fig. 3A shows characteristic ribbon-like assemblies. Fig. 3B is a height profile corresponding to the line drawn in the image in Fig. 3A. Each step corresponds to a 3.6 ± 0.4 nm height (Fig. 3C). Thus, the assemblies are composed of several layers of 3.6 nm ribbons.

Statistical analysis of their length and width shows that their length increased from 492 nm at $f_{tol} = 85.7$ v/v% to 1242 nm at $f_{tol} = 90.0$ v/v%, but their width remained constant at 82.0 ± 1 nm (Fig. 4A). Thus, the length-to-width ratio, R, increases from $R = 6.0$ at $f_{tol} = 85.7$ v/v% to $R = 15.2$ at $f_{tol} = 90.0$ v/v% (Fig. 4B). This indicates that increasing the toluene fractions further promotes a rapid anisotropic growth of the straight assemblies along their long axes. This corresponds to the accelerated gelation process, *i.e.*, t_{gel} decreases from 1300 to 2 min for $f_{tol} = 85.7$ v/v% to $f_{tol} = 90.0$ v/v% (Fig. 1).

The AFM height images in Fig. 5 show the assemblies within $93.0 \leq f_{tol} \leq 97.0$ v/v%. They are slightly different from those found within $85.7 \leq f_{tol} \leq 90.0$ v/v% (Fig. 3). Note that the height scales are 800 nm in Fig. 5A and 1000 nm in Fig. 5B and C. This is considerably larger than those shown in Fig. 3 because the assemblies become more complex and longer. This complexity comes from the twisted assemblies. Their length is, unfortunately, difficult to precisely measure. As shown in Fig. 5D, the enlarged image further outlines the contour characteristics of the aggregate structure. The assemblies also consist of thin, long, and twisted ribbons. The structural features are indicative of the formation of an intertwined 3D gel network of the assemblies.

The hierarchically assembled structures of the organogel at $f_{tol} = 100.0$ v/v% are different from those presented in Fig. 3 and

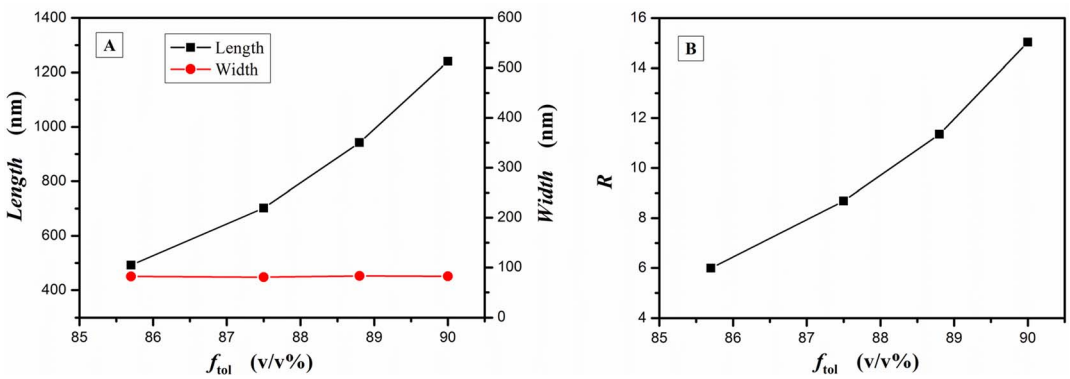

Fig. 4 Plots of the length and width (a) and the length-to-width ratio, R, (b) as a function of f_{tol} from 85 v/v% to 90.0 v/v%.

5. The AFM image in Fig. 6A shows a perfect 3D gel network formed by the twisted and intertwined assemblies. Analysis, as shown in Fig. 6B, indicates that the thin ribbons have a 5.0 ± 0.4 nm thickness (Fig. 6B and C) and a 100–180 nm width. The image also provides a picture regarding how the thin and twisted ribbons construct the 3D gel network through ribbon splitting and intertwining.

XRD characterization

The structures of the organogels were also characterized using X-ray diffraction. Fig. 7 shows the XRD patterns of the dried xerogel samples of the five organogels. There are two main diffraction signals: those within $2^\circ < 2\theta < 4^\circ$ and those within $5^\circ < 2\theta < 10^\circ$. The signal in $2^\circ < 2\theta < 4^\circ$ corresponds to a *d*-spacing value of about 3.5 nm related to a structure constructed by the entire hybrid molecule. The signals in $5^\circ < 2\theta < 10^\circ$ correspond to a *d*-spacing value of about 1.5 nm associated mainly with the ordered structure of the POM cluster.

For the sample at $f_{tol} = 100.0$ v/v%, the two diffraction peaks corresponds to $2\theta = 3.02^\circ$ and 6.0°. Their *d*-spacing values are $d_1 = 2.92$ and $d_2 = 1.47$ nm. The ratio of $d_1/d_2 = 1/2$ indicates a layered structure with a *d*-spacing value of 2.92 nm.[41] The other four samples at $f_{tol} = 95.0$, 90.0, 87.5, and 85.7 v/v% have a strong peak at $2\theta \approx 2.5^\circ$ to 3° and another strong and broad peak with a peak position at $2\theta \approx 6.5^\circ$. Their *d*-spacing values are 3.48, 3.34, 3.74, and 3.56 nm and 1.27, 1.21, 1.27, and 1.25 nm, respectively. The broad peaks can be split into at least three sub-peaks (Fig. S14 in the ESI†). The *d*-spacing values of 3.48, 3.34, 3.74, and 3.56 nm should correspond to a thickness of a layer structure similar to that found in the sample at $f_{tol} = 100.0$ v/v%. The *d*-spacing values of 1.27, 1.21, 1.27, and 1.25 nm are close to 1.2 nm diameter of the pristine POM cluster plus the three tetrabutyl ammonium cations.[37] This suggests that there is an orderly arrangement of the POM cluster within the ribbons.

Structure models

Based on these results, we suggest two models to schematically indicate the effect of the toluene/DMF ratio on the hierarchical structures formed during gelation (Scheme 2). In the conditions used here, the hybrid gelator assembled into ribbons during gelation. Within the ribbons, the POM cluster and the cholesterol parts in the gelator organized into a structure with an alternatively arranged POM layer and a cholesterol layer. The POM cluster and the cholesterol separate for free energy minimization. The ribbon thickness corresponds to the height measured using AFM, and the layer periodicity is the *d*-spacing measured with XRD. The chemical structure of the cholesterol–POM–cholesterol gelator and the size difference between the POM cluster and cholesterol suggest that the cholesterol is interdigitated. Thus, the *d*-spacing values are slightly greater than half of the total length (2.64 nm) of the gelator.

The difference between the two models is in the ordering of the POM clusters within the POM layer. In Type I, the POM clusters arrange orderly to maximize the POM cluster interactions. In this way, the ribbon becomes relatively straight and rigid. This model describes the structures of the ribbons that are formed in the gel within $85.7 \leq f_{tol} \leq 90.0$ v/v%. Alternatively, the POM clusters arrange slightly disorderly in Type II. Here, the ribbon becomes relatively twistable perhaps due to chirality of the cholesterol parts. This model describes the structure of the ribbons formed in the gel at $f_{tol} = 100.0$ v/v%. Rigidity or twistability of the ribbons was revealed by the AFM characterization (Fig. 2 and 6), and the ordering of the POM clusters was verified by the highest peak at $2\theta \approx 6.5^\circ$ (Fig. 7). For the gels within $90.0 \leq f_{tol} < 100.0$ v/v%, the structural features of the ribbons can be appropriately described by a mixed model consisting of the Type I and II models.

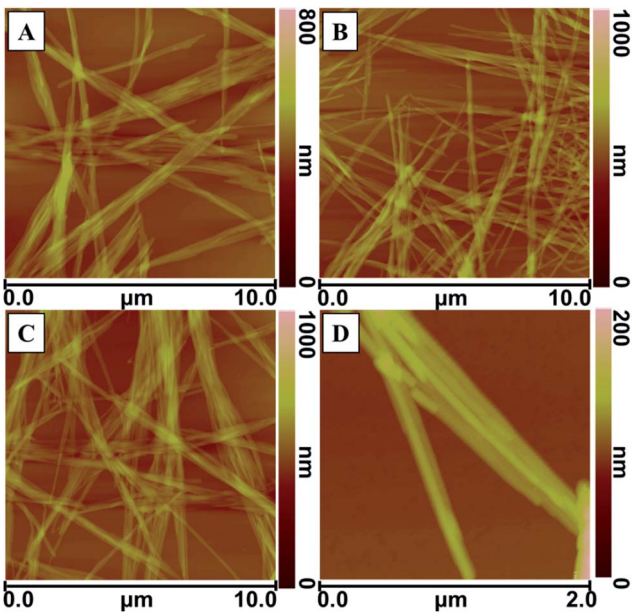

Fig. 5 AFM images of the dried xerogel samples of the organogels at $c = 10.0$ mg mL^{-1} and different f_{tol} values in the mixed solvents. (A) $f_{tol} = 93.0$ v/v%, (B) $f_{tol} = 95.0$ v/v%, and (C) $f_{tol} = 97.0$ v/v%. (D) An enlarged image of the sample at $f_{tol} = 95.0$ v/v% shows the fine structure.

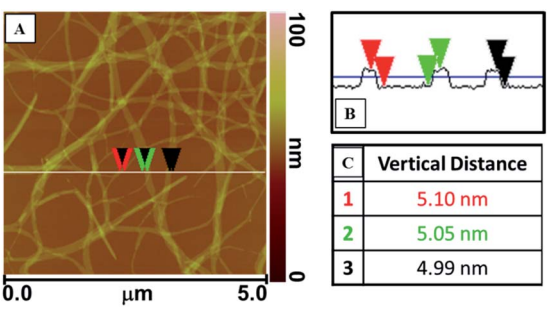

Fig. 6 (A) AFM image showing ribbon-like assemblies of the dried xerogel sample of the organogel at $f_{tol} = 100.0$ v/v%. The white line shows a section from which a height profile measurement was performed. (B) Height profile of the ribbons. (C) Vertical distance (or height) of the ribbons.

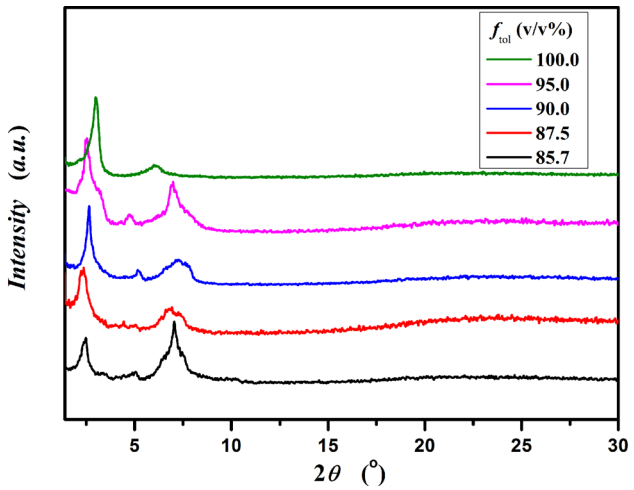

Fig. 7 XRD patterns of the dried xerogel samples of five organogels.

Balance between solubility and insolubility and the gelation process

As mentioned above, there is a delicate balance between the solvent–gelator interactions and gelator–gelator interactions. This balance plays an important role in determining the formation and growth of hierarchical structures as well as performances of the gels.[10] The gelation can be regulated by properly changing the toluene/DMF ratio because the nonpolar cholesterol parts and the polar POM cluster have a large difference in their solvent solubility in the mixed solvents. Naturally, the formation of the supramolecular structures is greatly associated with this change. Thus, the gel time is regulated by the properly changing toluene/DMF ratio.

At f_{tol} = 100.0 v/v%, the dielectric constant of the pure toluene is $\varepsilon^e = 2.24$. The good solubility of the hybrid gelator in toluene at 80 °C is mainly due to the interactions between the two cholesterol parts and the toluene molecules. When the hot solution is cooled to 23.0 °C, the contribution of such interaction to the solubility of the gelator is weakened. Because the POM cluster is insoluble in toluene, the gelator assembles into ribbons, and thus the solution becomes immobilized. Due to the poor solubility in toluene as well as its large size, the POM cluster ordering within the ribbons is poor. Thus, the gelation process of the hybrid gelator takes a long time.

For the solvent-mediated gelation processes, adding a certain amount of toluene into the DMF solutions to reach the predetermined c and f_{tol} also results in a significant variation in the solvent solubility. This variation corresponds a dielectric constant decrease from $\varepsilon^e = 36.71$ to a value at a fixed f_{tol}, for instance, $\varepsilon^e = 7.17$ for the mixed solvent with f_{tol} = 85.7 v/v%. Within 90.0 ≤ f_{tol} < 100.0 v/v%, the POM clusters no longer dissolve well in the mixed solvents, and thus this variation weakens the solvent–gelator interactions but strengthens the gelator–gelator interactions. In turn, the gelator assembles into ribbons. Once the ribbons form a 3D network, the solutions become immobilized.

Naturally, the gelation rate depends on the growth rate of ribbon-like assemblies. From f_{tol} = 85.7 v/v% to f_{tol} = 90.0 v/v%, the dielectric constant of the mixed solvents decreases from ε^e = 7.17 to ε^e = 5.68. This further strengthens the gelator–gelator interactions and thus could *positively* promote the arrangement of the gelators into ribbons. Therefore, the growth rate of the ribbons is increased, and the gelation rate increases as a function of f_{tol}.

With further decrease from ε^e = 5.68 to ε^e = 2.24 for f_{tol} = 90.0 v/v% to f_{tol} = 100.0 v/v%, further strengthening of the gelator–gelator interactions *negatively* promotes the arrangement of gelators onto aggregates. Apparently, the gelator–gelator interactions were strengthened. However, this promotion should not further maximize interactions between POM clusters because it also lowers gelator mobility. Thus, the growth rate of the ribbons slows down, and the gelation rate decreases with increasing f_{tol}.

Three-dimensional gel networks and rheological properties of gels

Thus far, we have characterized and discussed the formation of the two kinds of ribbons within two regimes of f_{tol}: 85.7 ≤ f_{tol} ≤ 90.0 v/v% and 90.0 ≤ f_{tol} ≤ 100.0 v/v%. Typically, the rigid and straight ribbons were found in the organolgel at f_{tol} = 90.0 v/v% (Fig. 3A), and the twisted ribbons were observed at f_{tol} = 100.0 v/v% (Fig. 6B). The ribbons build further the tertiary structures—the 3D gel networks (Scheme 3). At f_{tol} = 90.0 v/v%, rigid and straight ribbons construct the 3D gel network through a

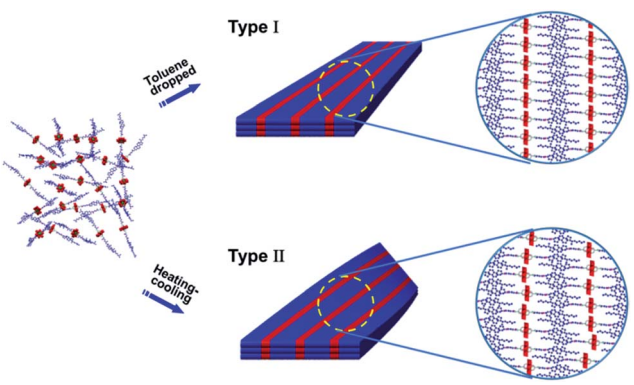

Scheme 2 Two models schematically represent the formation of the ribbons and the different arrangements of the hybrid gelator within the ribbons.

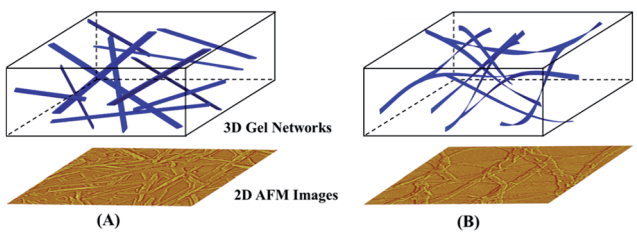

Scheme 3 Schematic representations of the two types of 3D gel networks with AFM amplitude images obtained from the dried sample of the organogels at f_{tol} = 90.0 (A) and 100.0 (B) v/v%.

"physical" connection between ribbons (Scheme 3A). At f_{tol} = 100.0 v/v%, the twisted ribbons construct the 3D gel network through ribbon splitting and intertwining (Scheme 3B). This network should be more perfect and consolidated than the former.

The rheological properties of gels are highly associated with the hierarchical structure, particularly the 3D gel network.[20,21,42–44] We also performed oscillatory rheology to characterize the dynamic shear storage and loss moduli (G' and G'') of our organogels under a strain sweep condition at 10.0 Hz. To better understand the organogels, we used two representative samples at c = 10.0 mg mL^{-1} at f_{tol} = 90.0 and 100.0 v/v% because of the large difference in their gel formation and hierarchical structure. Plots of the shear storage modulus, G', and the shear loss modulus, G'', as a function of strain ε^r are shown in Fig. 8. We can see that the two organogels show the same strain-amplitude dependence of the G' and G'' values within 0.01% ≤ ε^r ≤ 100%.

There are two critical strains, ε^r_{c1} and ε^r_{c2}, indicated by red and black arrows, respectively. Below ε^r_{c1}, G' and G'' slightly increase with increasing strain, which is known as strain hardening. Beyond it, they, particularly G', rapidly decrease with increasing strain to give a strain thinning behavior. Notably, when $G' > G''$ in $\varepsilon^r > \varepsilon^r_{c2}$, the gels are solid: however, when $G' < G''$ in $\varepsilon^r > \varepsilon^r_{c2}$, the gels are liquid. At this crossover point, $G' = G''$ corresponds to a change of behavior from a solid to a liquid. In other words, a gel-to-sol transition is caused by an external force. The differences between the organogels at f_{tol} = 90.0 and 100.0 v/v% are clear. The G' and G'' values of the organogel at f_{tol} = 100.0 v/v% are higher than those of the organogel at f_{tol} = 90.0 v/v%. ε^r_{c1} = 0.63% and ε^r_{c2} = 12.6% at f_{tol} = 100.0 v/v% are also higher than ε^r_{c1} = 0.40% and ε^r_{c2} = 4.0% at f_{tol} = 90.0 v/v%. This means that the organogel in the toluene solvent offers better rheological properties than those of the organogel in the mixed solvent. Evidently, this is because the toluene gel has better hierarchical structuring.

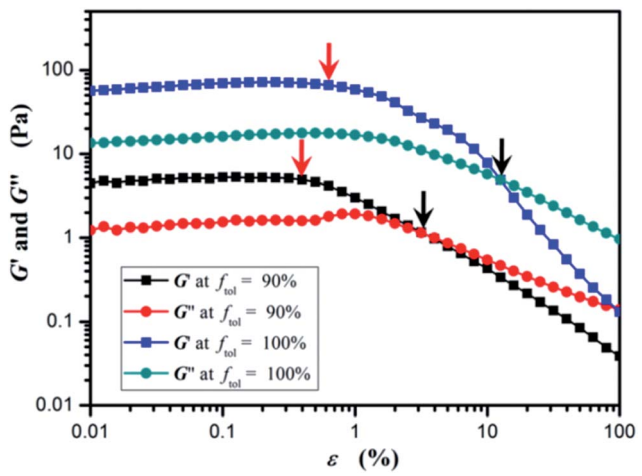

Fig. 8 Strain-amplitude dependences of the dynamic shear storage and loss moduli (G' and G'') of the two organogels at c = 10.0 mg mL^{-1} at f_{tol} = 90.0 and 100.0 v/v% at a constant frequency of 10.0 Hz. The red and black arrows point out two critical strains, ε^r_{c1} and ε^r_{c2}.

Conclusions

In summary, we found that the gel formation, supramolecular structures and performance of the organogels in the cholesterol–POM–cholesterol hybrid gelator within the toluene/DMF mixed solvents could be solvent-mediated. The novelty of this work is that by changing the toluene volume fraction, f_{tol}, in the mixed solvents, we can regulate solubility of this gelator. This is because the cholesterol dissolves in toluene and DMF, and the POM cluster dissolves in DMF. This solvent-mediated balance resulted in a V-shaped gelation process: the gelation time, t_{gel}, decreased from 1300 min to 2 min when f_{tol} increased from 85.7 v/v% to 90.0 v/v%, but it increased from 2 min to 5800 min when f_{tol} further increased from 90.0 v/v% to 100.0 v/v%.

Different ribbons formed in this system: a rigid and straight ribbon, in which the POM clusters arrange orderly within 85.7 ≤ f_{tol} ≤ 90.0 v/v%, and a twisted ribbon, in which the POM clusters arrange somewhat disorderly at f_{tol} = 100.0 v/v%. The orderly arrangement of the POM clusters promotes the ribbon growth rate, whereas the imperfect arrangement leads to a decrease in the ribbon growth rate. Thus, we observed that the V-shaped gelation rate varies as a function of f_{tol}. Furthermore, the rigid and straight ribbons constitute the 3D gel network through a "physical" connection between ribbons, whereas the twistable ribbons build up the 3D gel network *via* ribbon splitting and intertwining. Certainly, the latter network is stronger, and the gel presents better rheological properties than those of the former network. Our fundamental understanding will provide an efficient way to prepare organogels with this controllable gelation process and performances through a simple solvent-mediated route.

Acknowledgements

We appreciate the financial support of the National Natural Science Foundation of China for grants (Grant NSFC 21274069 and 21334003), PCSIRT (IRT1257), and Open Research Fund of State Key Laboratory of Polymer Physics and Chemistry, Changchun Institute of Applied Chemistry. We also thank Ms. Ellen Gao and Mr Eric Zhang for their assistances with the rheometrical experiments at Anton Paar Experimental Station (Beijing).

References

1 *Low Molecular Mass Gelators. Design, Self-Assembly, Function. Top. Current Chem.*, ed. F. Fages, Springer-Verlag Berlin, Berlin, 2005, vol. 256.
2 *Molecular Gels. Materials with Self-Assembled Fibrillar Networks*, ed. R. G. Weiss and P. Terech, Springer, Dordrecht, 2006.
3 P. Terech and R. G. Weiss, *Chem. Rev.*, 1997, **97**, 3133.
4 J. H. van Esch and B. L. Feringa, *Angew. Chem., Int. Ed.*, 2000, **39**, 2263.
5 L. A. Estroff and A. D. Hamilton, *Chem. Rev.*, 2004, **104**, 1201.
6 M. de Loos, B. L. Feringa and J. H. van Esch, *Eur. J. Org. Chem.*, 2005, 3615.

7 N. M. Sangeetha and U. Maitra, *Chem. Soc. Rev.*, 2005, **34**, 821.
8 P. Dastidar, *Chem. Soc. Rev.*, 2008, **37**, 2699.
9 A. R. Hirst, B. Escuder, J. F. Miravet and D. K. Smith, *Angew. Chem., Int. Ed.*, 2008, **47**, 8002.
10 J. H. van Esch, *Langmuir*, 2009, **25**, 8392.
11 A. Dawn, T. Shiraki, S. Haraguchi, S. I. Tamaru and S. Shinkai, *Chem.–Asian J.*, 2011, **6**, 266.
12 M.-O. M. Piepenbrock, G. O. Lloyd, N. Clarke and J. W. Steed, *Chem. Rev.*, 2010, **110**, 1960.
13 J. Y. Zhang and C. Y. Su, *Coord. Chem. Rev.*, 2013, **257**, 1373.
14 G.-Y. Zhu and J. S. Dordick, *Chem. Mater.*, 2006, **18**, 5988.
15 P. L. Zhu, X.-H. Yan, Y. Su, Y. Yang and J.-B. Li, *Chem.–Eur. J.*, 2010, **16**, 3176.
16 P.-H. Xue, R. Lu, X.-C. Yang, L. Zhao, D.-F. Xu, Y. Liu, H.-Z. Zhang, H. Nomoto, M. Takafuji and H. Ihara, *Chem.–Eur. J.*, 2009, **15**, 9824.
17 M. Bielejewski, A. Łapiński, R. Luboradzki and J. Tritt-Goc, *Langmuir*, 2009, **25**, 8274.
18 Y.-P. Wu, S. Wu, G. Zou and Q. J. Zhang, *Soft Matter*, 2011, **7**, 9177.
19 D. Dasgupta, S. Srinivasan, C. Rochas, A. Ajayaghosh and J. M. Guenet, *Soft Matter*, 2011, **7**, 9311.
20 N. Yan, Z.-Y. Xu, K. K. Diehn, S. R. Raghavan, Y. Fang and R. G. Weiss, *J. Am. Chem. Soc.*, 2013, **135**, 8989.
21 N. Yan, Z.-Y. Xu, K. K. Diehn, S. R. Raghavan, Y. Fang and R. G. Weiss, *Langmuir*, 2013, **29**, 793.
22 *Polyoxometalate Chemistry–From Topology via Self-Assembly to Applications*, ed. M. T. Pope and A. Müller, Kluwer Academic Publishers, Dordrecht, 2001.
23 Special thematic issue on polyoxometalates, *Chem. Rev.*, 1998, **98**, 1–388.
24 A. Proust, R. Thouvenot and P. Gouzerh, *Chem. Commun.*, 2008, 1837.
25 A. Dolbecq, E. Dumas, C. R. Mayer and P. Mialane, *Chem. Rev.*, 2010, **110**, 6009.
26 D. L. Long, R. Tsunashima and L. Cronin, *Angew. Chem., Int. Ed.*, 2010, **49**, 2.
27 P.-C. Yin, D. Li and T.-B. Liu, *Chem. Soc. Rev.*, 2012, **41**, 7368.
28 Y. Z. Wang, H. L. Li, C. Wu, Y. Yang, L. Shi and L. X. Wu, *Angew. Chem., Int. Ed.*, 2013, **52**, 4577.
29 Y. Yan, H. B. Wang, B. Li, G. F. Hou, Z. D. Yin, L. X. Wu and V. W. W. Yam, *Angew. Chem., Int. Ed.*, 2010, **49**, 9233.
30 S. Favette, B. Hasenknopf, J. Vaissermann, P. Gouzerh and C. Roux, *Chem. Commun.*, 2003, 2664.
31 M. Carraro, A. Sartorel, G. Scorrano, C. Maccato, M. H. Dickman, U. Kortz and M. Bonchio, *Angew. Chem., Int. Ed.*, 2008, **47**, 7275.
32 Y. L. Wang, W. Li and L. X. Wu, *Langmuir*, 2009, **25**, 13194.
33 Z. F. He, H. B. Wang, Y. L. Wang, Y. Wu, H. L. Li, L. H. Bi and L. X. Wu, *Soft Matter*, 2012, **8**, 3315.
34 Z. F. He, H. Ai, B. Li and L. X. Wu, *Chin. Sci. Bull.*, 2012, **57**, 4304.
35 B. Liu, J. Yang, M. Yang, Y. L. Wang, N. Xia, Z. J. Zhang, P. Zheng and W. Wang, *Soft Matter*, 2011, **7**, 2317.
36 H.-K. Yang, M.-M. Su, L.-J. Ren, P. Zheng and W. Wang, *RSC Adv.*, 2014, **4**, 1138.
37 H.-K. Yang, Y.-X. Cheng, M.-M. Su, Y. Xiao, M. B. Hu, W. Wang and Q. Wang, *Bioorg. Med. Chem. Lett.*, 2013, **23**, 1462.
38 J. E. Eldridge and J. D. Ferry, *J. Phys. Chem.*, 1954, **58**, 992.
39 B. Hasenknopf, R. Delmont, P. Herson and P. Gouzerh, *Eur. J. Inorg. Chem.*, 2002, 1081.
40 P. R. Marcoux, B. Hasenknopf, J. Vaissermann and P. Gouzerh, *Eur. J. Inorg. Chem.*, 2003, 2406.
41 C. Burger, S.-Q. Zhou and B. Chu, *Handbook of Polyelectrolytes and Their Applications*, ed. S. K. Tripathy, J. Kumar and H. S. Nalwa, American Scientific Publishers, 2002, vol. 3, p. 125.
42 J. Liu, P. L. He, J. L. Yan, X. H. Fang, J. X. Peng, K. Q. Liu and Y. Fang, *Adv. Mater.*, 2008, **20**, 2508.
43 J. L. Yan, J. Liu, P. Jing, C. K. Xu, J. M. Wu, D. Gao and Y. Fang, *Soft Matter*, 2012, **8**, 11697.
44 D. Gao, M. Xue, J.-X. Peng, J. Liu, N. Yan, P.-L. He and Y. Fang, *Tetrahedron*, 2010, **66**, 2961.

